Elementary Example of the Parametrization Method; Stable and Unstable Manifolds of the Standard Map.

J.D. Mireles James

October 25, 2007

Contents

1 Introduction:

This note presents an elementary example of the use of the so called Parametrization Method, which can be used to compute and prove the existence of invariant manifolds in dynamical systems. Several versions of the method are developed and applied in [HdlL1], [HdlL2], [HdlL6], [dlL3], [CFdlL4], [CFdlL5], [CFdlL5], and [BF].

The example worked here was chosen because it is of the simplest kind possible, allowing the method to be applied without the proliferation of technicalities.

Here the one dimensional stable and unstable manifolds of a hyperbolic fixed point of a planar diffeomorphism are computed. We give recursive relations for the coefficients of the power series of parametric functions whose image in the plane is an approximation of the manifolds. The approximation can be made as accurate as we like by varying the order of the truncated power series.

This is done by examining a functional relation which characterizes the invariant manifolds and their parameterizations. The methods used here are quite elementary. Nothing more than undergraduate mathematics is drawn upon, and very little of that. Nevertheless, the numerical results obtained are nontrivial. Working and writing up this problem has been an illuminating exercise and it is hoped that this note could prove of some value to a reader approaching these kinds of computations for the first time.

MatLab implementations of the numerical schemes described in the note are available at the authors web page:

www.math.utexas.edu/users/jjames/matLabPage.html

These MatLab files were used to produce all the graphics below.

We will be working with the standard map $f_\epsilon : \mathbb{T}^2 \to \mathbb{T}^2$ which is given by

$$f_\epsilon(x,\theta) = \begin{bmatrix} x + \epsilon \sin\theta & (mod 2\pi) \\ x + \theta + \epsilon \sin\theta & (mod 2\pi) \end{bmatrix} \tag{1}$$

For each $\epsilon > 0$ this is a diffeomorphism of the two torus with inverse

$$f_\epsilon^{-1}(x,\theta) = \begin{bmatrix} x - \epsilon \sin(\theta - x) & (mod 2\pi) \\ \theta - x & (mod 2\pi) \end{bmatrix}. \tag{2}$$

The map is an popular example in the study of area preserving dynamical systems. Its dynamics for various parameter values are reviewed in the appendix. The map can be thought of as a perturbation of a completely integrable area preserving map of the torus, and it clearly exhibits all the dynamical behavior associated with "Hamiltonian" maps, including persistence of primary and secondary tori, Birkhoff instability zones, homoclinic and heteroclinic dynamics about hyperbolic invariant sets (points in this case), and seperatrix splitting. At the same time the map is easy to write down and compute. We note that while the Arnold diffusion is not possible in this system (the invariant tori or circles have insides and outsides) the system can exhibit resonance hops. Area preserving maps, including the standard map, are discussed in more detail in [MH], and [R].

In the next section we catalog it's fixed points and review the linear analysis there. The linearized dynamics will be useful later in the note. Then we give the functional relations, develop there expansions, and find the recurrence relations

which solve them. Lastly some numerical application of the expansions are presented. The dynamics of the standard map are reviewed in the appendix. In the appendix we also look at some iterations of the parameterizations at a particular value of the parameter. These give a nice semi local picture of the homoclinic dynamics in the instability zone associated with the hyperbolic fixed point.

2 Fixed Points and Linear Analysis.

This section is a review the linear analysis of fixed points, and of numerical techniques that rely only on first order information. We find the fixed points of the standard map and examine their linear stability, giving the explicit formulas for their eigenvalues and eigenvectors. We recall the first order calculation of the stable and unstable manifolds of a fixed point. First order methods are commonly used in Engineering and Physics applications to compute these manifolds, and it will be of interest to compare these computations to the ones made later using higher order methods.

2.1 Eigenvalues and Eigenvectors.

While the material in this section is elementary, it will be convenient in later analysis to have explicit formulas for the fixed points, their differentials, and their eigenvalues and eigenvectors. Since these formula will be needed later and the thrust of the note is expository, we may as briefly review the relevant definitions and computations.

Fixed points of the standard map satisfy the equation

$$f_\epsilon(p) = p$$

for $p \in \mathbb{T}^2$ or $p = (x, \theta)$ both modulo 2π. This gives

$$\begin{bmatrix} x + \epsilon \sin\theta \\ x + \theta + \epsilon \sin\theta \end{bmatrix} = \begin{bmatrix} x \\ \theta \end{bmatrix}$$

which lead to the simultaneous equations

$$\epsilon \sin\theta = 0$$

$$x = -\epsilon \sin\theta$$

Then $\theta = 0$ or $\theta = \pi$ with $x = 0$ give the only fixed points. So letting p_0 and p_1 denote our fixed points we have

$$p_0 = (0, 0) \quad \text{and} \quad p_1 = (0, \pi)$$

both modulo 2π.

We are interested in the linearized map at the fixed points. Computing the differential we find that

$$Df(x,\theta) = \begin{bmatrix} 1 & \epsilon\cos\theta \\ 1 & 1+\epsilon\cos\theta \end{bmatrix}$$

so that $Df(p_0)$ and $Df(p_1)$ are

$$Df(0,0) = \begin{bmatrix} 1 & \epsilon \\ 1 & 1+\epsilon \end{bmatrix}$$

and

$$Df(0,\pi) = \begin{bmatrix} 1 & -\epsilon \\ 1 & 1-\epsilon \end{bmatrix}$$

.

Let $A = Df(p_i)$ with $i \in \{0,1\}$. In order to understand the linearized dynamics at these points we look for the eigenvalues and eigenvectors of these linear maps. Solving $Ax = \lambda x$ or

$$(A - \lambda I)x = 0 \tag{3}$$

At p_0 this the eigenvalue problem has non-zero solution if and only if $\det(A - \lambda I) = 0$, or

$$\det\begin{pmatrix} 1-\lambda & \epsilon \\ 1 & 1+\epsilon-\lambda \end{pmatrix} = 0$$

.

which gives the characteristic equation

$$\lambda^2 - (2+\epsilon)\lambda + 1 = 0. \tag{4}$$

Solving this gives eigenvalues

$$\begin{aligned} \lambda_1 &= 1 + \frac{\epsilon}{2} + \frac{\sqrt{\epsilon(4+\epsilon)}}{2} \\ \lambda_2 &= 1 + \frac{\epsilon}{2} - \frac{\sqrt{\epsilon(4+\epsilon)}}{2}. \end{aligned}$$

We estimate the magnitude of these by considering the quantity

$$\frac{\epsilon}{2} \pm \frac{\sqrt{\epsilon(4+\epsilon)}}{2} = 0.$$

Multiply these together to get

$$\left(\frac{\epsilon}{2} + \frac{\sqrt{\epsilon(4+\epsilon)}}{2}\right)\left(\frac{\epsilon}{2} - \frac{\sqrt{\epsilon(4+\epsilon)}}{2}\right) = \frac{\epsilon^2}{4} - \frac{\epsilon(4+\epsilon)}{4} = \frac{-\epsilon}{4} < 0$$

for $\epsilon > 0$. Since the product is negative for all positive epsilon the terms have opposite signs. Since one is less than zero and one is greater than zero, we have one eigenvalue larger than one and one smaller than one. But clearly

$$\lambda_1 = 1 + \frac{\epsilon}{2} + \frac{\sqrt{\epsilon(4+\epsilon)}}{2}$$

is larger than one for all $\epsilon > 0$. Then

$$\lambda_2 = 1 + \frac{\epsilon}{2} - \frac{\sqrt{\epsilon(4+\epsilon)}}{2}.$$

is less than one for all $\epsilon > 0$ and we have a hyperbolic pair of eigenvalues.

In summary p_0 is a hyperbolic fixed point for all $\epsilon > 0$.

To find the eigenvectors we solve

$$\begin{pmatrix} (1-\lambda) & \epsilon \\ 1 & 1+\epsilon-\lambda \end{pmatrix} \begin{bmatrix} \xi_1 \\ \xi_2 \end{bmatrix} = \begin{bmatrix} 0 \\ 0 \end{bmatrix}$$

which gives

$$\xi_2 = \xi_1 \left(\frac{1}{2} \pm \frac{\sqrt{\epsilon(4+\epsilon)}}{2\epsilon}\right)$$

with ξ_1 arbitrary.

Similarly, at p_1 we have the condition

$$\det \begin{pmatrix} 1-\lambda & -\epsilon \\ 1 & 1-\epsilon-\lambda \end{pmatrix} = 0$$

.

$$\lambda^2 + (\epsilon - 2)\lambda + 1 = 0$$

and have eigenvalues

$$\lambda_{1,2} = 1 - \frac{\epsilon}{2} \pm \frac{\sqrt{\epsilon(\epsilon-4)}}{2} = \frac{2-\epsilon}{2} \pm i\frac{\sqrt{\epsilon(4-\epsilon)}}{2}$$

for $0 < \epsilon < 4$. Then solving

$$\begin{pmatrix} (1-\lambda) & -\epsilon \\ 1 & 1-\epsilon-\lambda \end{pmatrix} \begin{bmatrix} \xi_1 \\ \xi_2 \end{bmatrix} = \begin{bmatrix} 0 \\ 0 \end{bmatrix}$$

gives the complex eigenvectors

In this set of notes we are interested only in the hyperbolic fixed point p_0 as this can be treated by elementary methods, essentially using little more than undergraduate mathematics. The aim of the note is to develop power series representations of the stable and unstable manifolds of p_0. The problem of computing invariant circles near the fixed point at p_1 for $\epsilon > 0$ leads to the problem small divisors. It's essentially a KAM problem which in fact can be solved by the parametrization method.

Before introducing the parametrization method for the stable and unstable manifolds of p_0, we pause to consider the usual linear computation of these objects.

2.2 Linear Analysis of Stable and Unstable Manifolds.

Recall that by the Hartman-Gorbman there exists an neighborhood V about the hyperbolic fixed point p_0 so that the dynamics of the standard map are topologically conjugate to the dynamics of it's linearization. See [R] for the general statement and proof. Then, in some small enough neighborhood of p_0 there is a topological line of points which converge to p_0 under iteration of the standard map, and a separate line of points which converge to p_0 under iteration of it's inverse.

Moreover, by the stable manifold theorem for a hyperbolic fixed point, the line is not only topological, but as smooth as the map; in this case analytic. See again [R] for statement and proof (as an timely aside, note that this stable manifold theorem, as well as many far-reaching generalizations can in fact be proved by the parametrization method. See [HdlL6], [CFdlL4], [CFdlL5], and [CFdlL5]).

Global versions of the theorem state that the stable and unstable manifolds exist beyond the neighborhood V given by Hartman-Gorbman; globally they are immersed submanifolds. Note that they may not be embedded. In fact many examples and theorems (say for example the homoclinic tangle theorem that will be discussed later) show that the immersion need not be neat.

On the other hand, there are many applications where we may want as much information as possible about the global immersion of the manifolds. Stable and unstable manifolds tend to organize the dynamics in chaotic regions of phase space. Understanding how they are immersed plays a key role in theoretical investigations of chaotic behavior. The mathematical literature is too rich to do justice to on this mater. Some examples are [GR1], [GR2], and [GdlL]. The reader might consult references in these papers for a more complete view of the literature.

In physical applications it could happen that the fixed point is a destination, say for a mission design problem in Celestial Mechanics. Then the stable manifold is the set of all points in the phase space which reach this destination under the natural dynamics of the system (no maneuvers necessary), and the unstable manifold is the set of all points that can be reached leaving the fixed point with an arbitrarily small velocity (maneuver as small as you like). See for example [K1], and [K2] as well as the references therein for many other applications.

For these reasons and many more there has been (since say Poincare) much interest in methods for computing stable and unstable manifolds. The easiest method, and one which is often used, is to combine linear analysis of the fixed points with the fact that the stable and unstable manifolds are tangent to the stable and unstable eigenvectors at the fixed point (this is part of the conclusion of the local stable/unstable manifold theorem). Then the eigenvectors give the best linear approximation of the manifolds, near the fixed point.

So lets suppose we want to approximate the stable and unstable manifolds emanating from the fixed point p_0 of the standard map. We have exact expressions for the stable and unstable eigenvectors there. Then we can simply choose a grid of points near the origin and on the line determined by these vectors.

The points are in the tangent space of the stable and unstable manifolds, so if we stay close enough to the point p_0, we expect they should be very approximately on the stable and unstable manifolds. Now if we iterate the points on the unstable eigenvector by the standard map, and iterate the points on the stable eigenvector by it's inverse, the resulting trajectories should lie close to the stable and unstable manifolds.

Several questions arise. How close to the origin do we have to start this procedure? For how many iterates can we expect the approximation to be good? What should we mean by "good" in this setting? We will return to these questions later. However if one indulges in a little trial and error, quite nice results can be obtained quickly and with little effort.

As a first example see figure 1. Here we consider the standard map with $\epsilon = 1.3$. We scale the eigenvectors down to a magnitude of 10^{-7}, and take 1000 points along each of them. The points are themselves 10^{-7} apart. This initial grid of points is iterated twelve times (points on the stable eigenvector are iterated by f^{-1} and points on the unstable manifold iterated by f). The stable manifold is shown in red and the unstable in green (since the phase space is $\mathbb{T}^2$ the corners of the square are identified with p_0).

How much faith can we place in the resulting figure? To measure this we choose the last point in our approximation of the stable manifold, and iterate it under f. If the point approximates well a point on the stable manifold, then we expect it to converge under forward iterations to the fixed point.

The orbit of the point is shown in 1. The initial condition is at roughly $x = 0.7, \theta = 0.2$ in the lower left hand corner of the figure, and is enclosed in a red circle. By looking back at figure 1 its clear that this is where the green curve stopped. The point is iterated and we see it converging to the upper left corner.

Figure 3 quantifies the convergence. The x-axis of the figure is the number

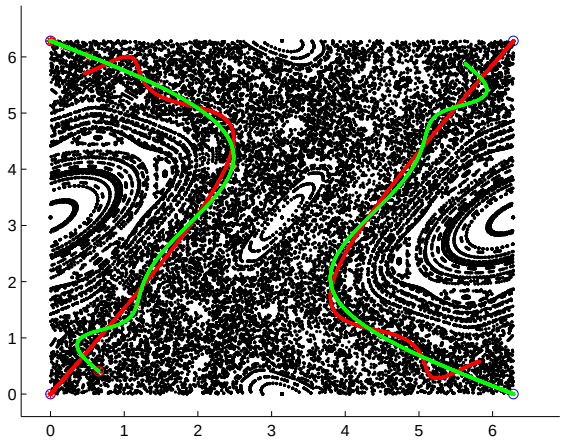

Figure 1: Linear Computation of Stable and Unstable Manifolds.

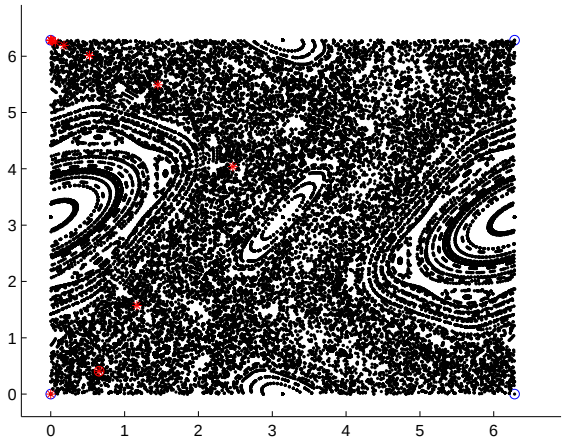

Figure 2: Orbit of the last point on the approximation of $W^s(p_0)$.

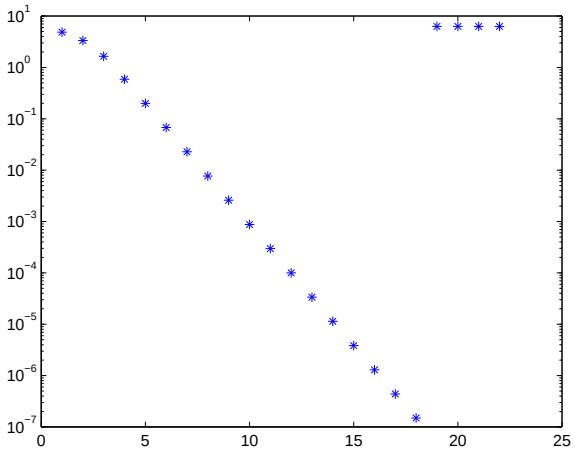

Figure 3: Distance of the orbit from p_0.

of iterates and the y-axis is the distance from p_0 in a logarithmic scale. Its clear that the orbit moves toward the fixed point for 18 iterations, coming within a distance of 10^{-7} of the fixed point, before numerical perturbations push it off the manifold and it moves away. Since the point was iterated away from the fixed point twelve times, the fact that is stays on the manifold for eighteen iterates is a good sign that the approximation is usefull.

As an extreme example in the other direction consider figure 4. Here we begin with the same initial conditions as before, but iterate three hundred times. We see that the approximation to the manifolds obtained fills the better part of the Birkhoff instability zone.

We ask the same question as before; Can we trust the approximation at this point? Perhaps the answer is yes. There are reasons to believe that the stable and unstable manifolds eventually pass near every point in the phase space that they "can". For example, in the plane the invariant tori about the elliptic fixed point and the tori about other resonance points will keep the stable and unstable manifolds away from these points for all time. But if the Birkhoff zone is mixing (as one expects) then eventually we expect the immersion of $W^s(p_0)$ and $W^u(p_0)$ to fill the region densely.

So we repeat the previous analysis. We choose the last point in our approximation of the stable manifold, and iterate it three hundred times. The orbit is shown in figure 5. The orbit seems to wander around the tori about p_1, but we never see any clear piling up near p_0.

Again this is quantified in figure 6. The y axis is logarithmic again and we see that in four hundred and fifty iterates the orbit never comes notably close to the fixed point, and certainly never accumulates there. So the orbit is in fact

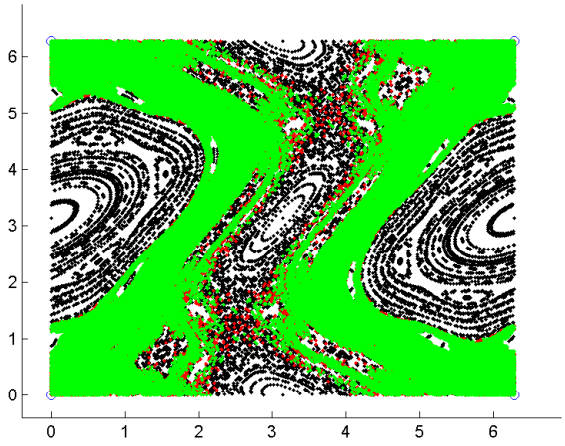

Figure 4: Another Computation of Stable and Unstable Manifolds.

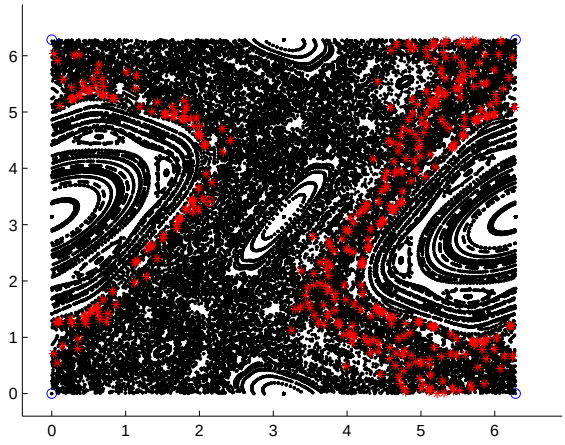

Figure 5: Linear Computation of Stable and Unstable Manifolds.

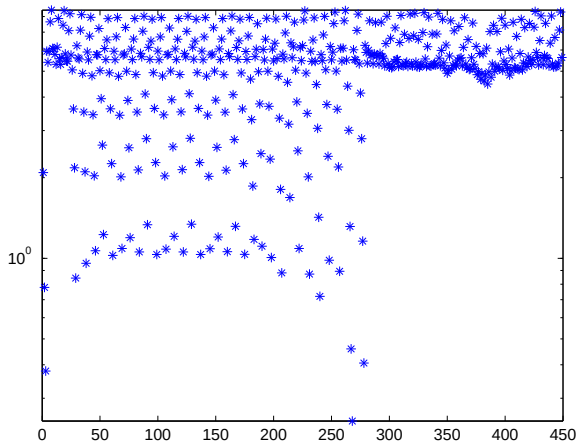

Figure 6: Linear Computation of Stable and Unstable Manifolds.

off the stable manifold and the approximation is useless at this point.

Of course the approximation works well for many more than twelve iterations and breaks down somewhere before three hundred iterations. It is not the goal of this note to make a detailed study of this method. We simply note that it can be done, and that it can yield excellent results, although some trial and error may be necessary, and it may not be clear how to choose optimal parameters (how many points to begin with, or how close they should be to the fixed point). It will turn out that the parametrization method will shed some light on even this first order method. Before returning to this comment, we introduce the method.

3 Parametrization Method for the Hyperbolic Fixed Point.

This section begins the study of the parametrization method. After introducing the method formally we are able, in this simple planar case, to write down explicitly the recursion relations for the coefficients of a pair of power series which, taken as a parametric function, give the stable/unstable manifolds of the fixed point at the origin.

3.1 Invariance Equations and Expansions

What we want to do is represent as large a piece of $W^u(p_0)$ or $W^s(p_0)$ as possible by a parametric function P from an open interval $U \subset \mathbb{R}$ into $\mathbb{T}^2$, the phase

space of the standard map. In that case we would have $f_\epsilon(P(U)) \subset P(U)$ for the stable manifold, and $P(U) \subset f_\epsilon(P(U))$ for the unstable. We also want to find a function λ from the parameter space into itself which describes the dynamics on the manifold.

To be precise, we seek P and λ such that the following diagram to commutes

$$\begin{array}{ccc} \mathbb{T}^2 & \stackrel{f_\epsilon}{\longrightarrow} & \mathbb{T}^2 \\ P \uparrow & & \uparrow P \\ U \subset \mathbb{R} & \stackrel{\longrightarrow}{\lambda} & U \subset \mathbb{R} \end{array}$$

or equivalently, we solve the invariance equation

$$f_\epsilon \circ P = P \circ \lambda \tag{5}$$

with $P : \mathbb{R} \to \mathbb{T}^2$ and $\lambda : \mathbb{R} \to \mathbb{R}$.

To begin we take $P(t) = (x(t), \theta(t))$ and look for $\{a_n\}, \{b_n\}$ such that

$$x(t) = \sum_{n=0}^{\infty} a_n t^n$$

and

$$\theta(t) = \sum_{n=0}^{\infty} b_n t^n$$

solve the invariance equation, subject to the assumption that $\lambda : \mathbb{R} \to \mathbb{R}$ is a linear map, and hence a constant $\lambda \in \mathbb{R}$ (i.e. we want the dynamics in the parameter space to be in "normal form" or to be "as simple as possible". It may not be possible in all cases one ever encounters to take λ linear. However in the case of a hyperbolic fixed point in finite dimension this can always be done. Here we will prove that λ can be taken as linear simply by showing that it works).

Inserting these into the invariance equations for the standard map gives

$$\left[\begin{array}{c} x(t) + \epsilon \sin \theta(t) \\ x(t) + \theta(t) + \epsilon \sin \theta(t) \end{array} \right] = \left[\begin{array}{c} x(\lambda(t)) \\ \theta(\lambda(t)) \end{array} \right] \tag{6}$$

or say

$$(f_\epsilon \circ P)(t) = f_\epsilon \circ \left(\sum_{n=0}^{\infty} a_n t^n, \sum_{n=0}^{\infty} b_n t^n \right) = \left(\sum_{n=0}^{\infty} a_n (\lambda(t))^n, \sum_{n=0}^{\infty} b_n (\lambda(t))^n \right) = (P \circ \lambda)(t).$$

Combining the previous expressions with the fact that λ is to be constant, give

$$\left[\begin{array}{c} \sum_{n=0}^{\infty} a_n t^n + \epsilon \sin \left(\sum_{n=0}^{\infty} b_n t^n \right) \\ \sum_{n=0}^{\infty} a_n t^n + \sum_{n=0}^{\infty} b_n t^n + \epsilon \sin \left(\sum_{n=0}^{\infty} b_n t^n \right) \end{array} \right] = \left[\begin{array}{c} \sum_{n=0}^{\infty} a_n \lambda^n t^n \\ \sum_{n=0}^{\infty} b_n \lambda^n t^n \end{array} \right] \tag{7}$$

or

$$\sum_{n=0}^{\infty} a_n t^n + \epsilon \sum_{j=0}^{\infty} \frac{(-1)^j}{(2j+1)!} \left[\sum_{n=0}^{\infty} b_n t^n \right]^{2j+1} = \sum_{n=0}^{\infty} a_n \lambda^n t^n$$

$$\sum_{n=0}^{\infty} a_n t^n + \sum_{n=0}^{\infty} b_n t^n + \epsilon \sum_{j=0}^{\infty} \frac{(-1)^j}{(2j+1)!} \left[\sum_{n=0}^{\infty} b_n t^n \right]^{2j+1} = \sum_{n=0}^{\infty} b_n \lambda^n t^n$$

What is required is that we expand both sides and match powers of t.

Before we attempt to write down the general recursion relations for the coefficients $\{a_n\}$ and $\{b_n\}$ lets consider the zeroth and first order terms. Expanding to first order one has

$$a_0 + a_1 t + \ldots + \epsilon \left(b_0 + b_1 t + \ldots\right) + \frac{\epsilon}{3!} \left(b_0 + b_1 t + \ldots\right)^3 + \ldots = a_0 + a_1 \lambda t + \ldots$$

$$a_0 + a_1 t + \ldots + b_0 + b_1 t + \ldots + \epsilon \left(b_0 + b_1 t + \ldots\right) + \frac{\epsilon}{3!} \left(b_0 + b_1 t + \ldots\right)^3 + \ldots = b_0 + b_1 \lambda t + \ldots$$

From the first equation

$$a_0 + \epsilon b_0 + \frac{\epsilon}{3!} b_0^3 + \ldots = a_0$$

or

$$\epsilon b_0 + \frac{\epsilon}{3!} b_0^3 + \ldots = \epsilon \sin(b_0) = 0$$

so that $b_0 = 0 \mod 2\pi$. Plugging this into the second equation gives $a_0 + \ldots = 0 * a_0 + b_0 + \ldots$, so that both zero order terms vanish and

$$a_0 = 0 \quad \text{and} \quad b_0 = 0$$

both mod 2π. Then the parametrization vanishes at $t = 0$, so that it's graph contains the origin. Certainly we would require at least this form a proper solution. It's only noteworthy that we did not have to impose it externally. Even if we proceeded blindly, the invariance equation give the condition.

Moving on to first orders of t and using that the constant terms are zero gives gives

$$a_1 t + \epsilon b_1 t = a_1 \lambda t$$

$$a_1 t + (1 + \epsilon) b_1 t = b_1 \lambda t$$

as $\sum b_n t^n$ to a power k will have leading term of order at least k, due to the fact that $b_0 = 0$. Better still we write this as

$$\begin{bmatrix} a_1 + \epsilon b_1 \\ a_1 + (1+\epsilon) b_1 \end{bmatrix} = \begin{bmatrix} \lambda a_1 \\ \lambda b_1 \end{bmatrix} \tag{8}$$

which is to say

$$\begin{bmatrix} 1 & \epsilon \\ 1 & (1+\epsilon) \end{bmatrix} \begin{bmatrix} a_1 \\ b_1 \end{bmatrix} = \lambda \begin{bmatrix} a_1 \\ b_1 \end{bmatrix}. \tag{9}$$

Noting that the matrix is $Df_\epsilon(0,0)$ we have that (a_1, b_1) is an eigenvector of the differential of f at the fixed point. We also obtain that the linear dynamics $\lambda : \mathbb{R} \to \mathbb{R}$ in the parameter space are given by the eigenvalues of $Df_\epsilon(0,0)$.

This agrees with the fact that $W^u(0,0)$ and $W^s(0,0)$ should be tangent to the stable and unstable eigenspaces and that the dynamics in the manifolds, near the origin, should be conjugate to the linear dynamics (stable/unstable manifold theorem and Hartman-Gorbman). Again, we did not have to impose these. We simply follow the invariance equations. (This begins to suggest how this method could be used to give independent proof of the stable manifold theorem).

Recalling the formulas from the previous section one has that

$$\lambda = 1 + \frac{\epsilon}{2} \pm \frac{\sqrt{\epsilon(4+\epsilon)}}{2}$$

and

$$b_1 = a_1 \left(\frac{1}{2} \pm \frac{\sqrt{\epsilon(4+\epsilon)}}{2\epsilon} \right)$$

with a_1 arbitrary. Then if we pick the stable eigenvalue, the dynamics in the parameter space will push any initial condition $t_0 \in \mathbb{R}$ to zero. Passing through the invariance equations, this implies that $P(t_0) \in \mathbb{T}^2$ will converge under forward iteration to $(0,0) = p_0$, so that by definition $P(t_0)$ is on the stable manifold. Similarly for the unstable eigenvalue. Then choosing to insert the stable eigenvalue and eigenvector into the previous computations gives the parametrization of the stable manifold to order one, and similarly for the unstable eigenvalue and eigenvector.

By continuing these computations, expanding the third and fifth order terms of the sin function, the coefficients up to fifth order can be obtained by hand. The patient reader can check that this gives that $a_2 = b_2 = a_4 = b_4 = 0$ and that the third and fifth order terms solve

$$\begin{bmatrix} 1-\lambda^3 & \epsilon \\ 1 & (1+\epsilon-\lambda^3) \end{bmatrix} \begin{bmatrix} a_3 \\ b_3 \end{bmatrix} = \frac{\epsilon}{3!} \begin{bmatrix} b_1^3 \\ b_1^3 \end{bmatrix}. \tag{10}$$

and

$$\begin{bmatrix} 1-\lambda^5 & \epsilon \\ 1 & (1+\epsilon-\lambda^5) \end{bmatrix} \begin{bmatrix} a_5 \\ b_5 \end{bmatrix} = \epsilon \begin{bmatrix} \frac{3b_1^2 b_3}{3!} - \frac{b_1^5}{5!} \\ \frac{3b_1^2 b_3}{3!} - \frac{b_1^5}{5!} \end{bmatrix}. \tag{11}$$

An induction shows that $x(t)$ and $\theta(t)$ are odd functions.

Now we want to find the coefficients up to arbitrary order. We would like a more efficient way to compute the recursion relations, as expanding all terms of the sine function up to order n will give an n-th order recursion. If one is just a little more thoughtful the recursion can be reduced to order 2. This is the subject of the the next section.

3.2 Recurrence Relations.

In order to get efficient recursion we have to deal with the nonlinearity. In general the composition of two power series will lead to involved combinatorial relations among the coefficients. However if the outer function satisfies some simple differential equation there is a trick which can reduce complications significantly. The trick is developed in Knuth [Kun] where he uses it to compute the power series of V^α with V a known power series. However it is claimed there that the trick goes back at least to Euler.

Let

$$W(t) = \sum_{n=0}^{\infty} \beta_n t^n = \sin(\theta(t)) = \sin\left(\sum_{n=0}^{\infty} b_n t^n\right)$$

As usual, when dealing with the sine and cosine functions it is desirable to complexify and work with the exponential. Then let

$$\bar{W}(t) = \sum_{n=0}^{\infty} (\alpha_n + i\beta_n) t^n = e^{i\theta(t)}$$

so that $W(t) = Im(\bar{W}(t))$

Differentiating we have

$$\bar{W}'(t) = ie^{i\theta(t)}\theta'(t)$$

into which we insert the definition of $\bar{W}$ to obtain the relation

$$\bar{W}'(t) = i\bar{W}(t)\theta'(t)$$

Expanding in powers of t gives

$$\sum_{n=0}^{\infty} (n+1)(\alpha_{n+1}+i\beta_{n+1}) t^n = i\left[\sum_{n=0}^{\infty} (\alpha_n + i\beta_n) t^n\right]\left[\sum_{n=0}^{\infty} (n+1) b_{n+1} t^n\right] = i\sum_{n=0}^{\infty} c_n t^n$$

with

$$c_n = \sum_{k=0}^{n} (k+1)(\alpha_{n-k} + i\beta_{n-k})b_{k+1}$$

by the usual convolution formula for the product of power series. Then

$$\sum_{n=0}^{\infty} [(n+1)\alpha_{n+1} + i(n+1)\beta_{n+1}]t^n =$$

$$\sum_{n=0}^{\infty} i \left[\sum_{k=0}^{n} (\alpha_{n-k} + i\beta_{n-k})(k+1)b_{k+1} \right] t^n =$$

$$\sum_{n=0}^{\infty} \left(-\sum_{k=0}^{n} (k+1)\beta_{n-k}b_{k+1} + i \sum_{k=0}^{n} (k+1)\alpha_{n-k}b_{k+1} \right) t^n$$

Taking real and imaginary parts yields

$$\sum_{n=0}^{\infty} (n+1)\,\alpha_{n+1}t^n = \sum_{n=0}^{\infty} \left(-\sum_{k=0}^{n} (k+1)\,\beta_{n-k}b_{k+1} \right) t^n$$

$$\sum_{n=0}^{\infty} (n+1)\,\beta_{n+1}t^n = \sum_{n=0}^{\infty} \left(\sum_{k=0}^{n} (k+1)\,\alpha_{n-k}b_{k+1} \right) t^n.$$

Finally, equating like powers gives

$$(n+1)\,\alpha_{n+1} = -\sum_{k=0}^{n} (k+1)\,\beta_{n-k}b_{k+1}$$

$$(n+1)\,\beta_{n+1} = \sum_{k=0}^{n} (k+1)\,\alpha_{n-k}b_{k+1}$$

which we solve for α_{n+1} and β_{n+1} to obtain the recurrence relations

$$\alpha_{n+1} = \frac{-1}{n+1} \sum_{k=0}^{n} (k+1)\,\beta_{n-k}b_{k+1}$$

$$\beta_{n+1} = \frac{1}{n+1} \sum_{k=0}^{n} (k+1)\,\alpha_{n-k}b_{k+1}$$

and we are ready to compute

$$\sin(\theta(t)) = \sum_{n=0}^{\infty} \beta_n t^n$$

to any order in terms of the coefficients b_n of $\theta(t)$.

This is something of a miracle, and a trick worth remembering. The power series of sine and cosine (or say the exponential) involve all powers of the dependant variable. One puts a second power series into this mess and can nevertheless obtain recursions that are no more complex than the convolution formula.

In other words, you are told it will be necessary to compute $(\sum a_n t^n)^k$ for all powers of k. You shuffle a few symbols around and find instead that the resulting computation is no worse than the computation of $(\sum a_n t^n)^2$. This is a strong reminder that if your problem hands you functional relations, you are wise to use them (the parametrization method is another example of this, as are numerical methods such as the so called 'high order Taylor method' which are based on this kind of 'automatic differentiation').

To begin the recursion we need the base cases

$$\begin{aligned}\bar{W}(0) = \alpha_0 + i\beta_0 &= \cos(\theta(0)) + i\sin(\theta(0)) \\ &= \cos(b_0) + i\sin(b_0) \\ &= \cos(0) + i\sin(0) \\ &= 1\end{aligned}$$

so that

$$\alpha_0 = 1 \quad \text{and} \quad \beta_0 = 0.$$

Now we are ready to take up the recursion for a_n and b_n.

Beginning with

$$x(t) + \epsilon\sin(\theta(t)) = x(\lambda t)$$

$$x(t) + \theta(t) + \epsilon\sin(\theta(t)) = \theta(\lambda t)$$

we have

$$\sum_{n=1}^{\infty} a_n t^n + \epsilon \sum_{n=1}^{\infty} \beta_n t^n = \sum_{n=1}^{\infty} a_n \lambda^n t^t$$

$$\sum_{n=1}^{\infty} a_n t^n + \sum_{n=1}^{\infty} b_n t^n + \epsilon \sum_{n=1}^{\infty} \beta_n t^n = \sum_{n=1}^{\infty} b_n \lambda^n t^t$$

or

$$\sum_{n=1}^{\infty}[1-\lambda^n]\,a_n\,t^n = -\epsilon\sum_{n=1}^{\infty}\beta_n t^n$$

$$\sum_{n=1}^{\infty}[a_n + (1-\lambda^n)b_n]t^n = -\epsilon\sum_{n=1}^{\infty}\beta_n t^n.$$

Equating like powers gives

$$(1-\lambda^{n+1})a_{n+1} = -\epsilon\beta_{n+1}$$

$$a_{n+1} + (1-\lambda^{n+1})b_{n+1} = -\epsilon\beta_{n+1}.$$

Recalling the recurrence for β_{n+1} one finds

$$(1-\lambda^{n+1})a_{n+1} = \frac{-\epsilon}{n+1}\sum_{k=0}^{n}(k+1)\,\alpha_{n-k}b_{k+1}$$

$$a_{n+1} + (1-\lambda^{n+1})b_{n+1} = \frac{-\epsilon}{n+1}\sum_{k=0}^{n}(k+1)\,\alpha_{n-k}b_{k+1}$$

and interestingly enough we have dependance on α_n instead of β_n.

Observe that the n^{th} term in the sum only contains b_{n+1};

$$\frac{-\epsilon}{n+1}\sum_{k=0}^{n}(k+1)\,\alpha_{n-k}b_{k+1} = \frac{-\epsilon\,(n+1)}{n+1}\alpha_0 b_{n+1} + \frac{-\epsilon}{n+1}\sum_{k=0}^{n-1}(k+1)\,\alpha_{n-k}b_{k+1}$$

$$= -\epsilon b_{n+1} + \frac{-\epsilon}{n+1}\sum_{k=0}^{n-1}(k+1)\,\alpha_{n-k}b_{k+1}$$

as $\alpha_0 = 1$.

Moving the b_{n+1} term to the left hand side of the equations for the $n+1$ power of t above gives

$$(1-\lambda^{n+1})a_{n+1} + \epsilon b_{n+1} = \frac{-\epsilon}{n+1}\sum_{k=0}^{n-1}(k+1)\,\alpha_{n-k}b_{k+1}$$

$$a_{n+1} + (1+\epsilon-\lambda^{n+1})b_{n+1} = \frac{-\epsilon}{n+1}\sum_{k=0}^{n-1}(k+1)\,\alpha_{n-k}b_{k+1}$$

or

$$\left[\begin{array}{cc} 1-\lambda^{n+1} & \epsilon \\ 1 & 1+\epsilon-\lambda^{n+1} \end{array}\right]\left[\begin{array}{c} a_{n+1} \\ b_{n+1} \end{array}\right] = \frac{-\epsilon}{n+1}\sum_{k=0}^{n-1}(k+1)\,\alpha_{n-k}b_{k+1}\left[\begin{array}{c} 1 \\ 1 \end{array}\right].$$

which is infinitely many linear systems of two equations in two unknowns. In two dimensions it is easy to invert the matrix symbolically to obtain

$$\left[\begin{array}{c} a_{n+1} \\ b_{n+1} \end{array}\right] = \left(\frac{-\epsilon}{n+1}\sum_{k=0}^{n-1}(k+1)\,\alpha_{n-k}b_{k+1}\right)A^{-1}\left[\begin{array}{c} 1 \\ 1 \end{array}\right].$$

where

$$A^{-1} = \frac{1}{(1-\lambda^{n+1})(1+\epsilon-\lambda^{n+1})-\epsilon}\left[\begin{array}{cc} 1+\epsilon-\lambda^{n+1} & -\epsilon \\ -1 & 1-\lambda^{n+1} \end{array}\right].$$

The matrix is invertable as $\lambda^n \neq \lambda$ for $n \geq 2$ (the eigenvalues are the unique numbers that give a nontrivial kernal). The results will look nicer if we abandon the matrix notation. Then summarizing the results of the section we have

$$a_{n+1} = \frac{-\epsilon(1-\lambda^{n+1})}{(n+1)[(1-\lambda^{n+1})(1+\epsilon-\lambda^{n+1})-\epsilon]}\sum_{k=0}^{n-1}(k+1)\,\alpha_{n-k}b_{k+1}$$

$$b_{n+1} = \frac{\epsilon\lambda^{n+1}}{(n+1)[(1-\lambda^{n+1})(1+\epsilon-\lambda^{n+1})-\epsilon]}\sum_{k=0}^{n-1}(k+1)\,\alpha_{n-k}b_{k+1}$$

with

$$\alpha_{n+1} = \frac{-1}{n+1}\sum_{k=0}^{n}(k+1)\,\beta_{n-k}b_{k+1}$$

$$\beta_{n+1} = \frac{1}{n+1}\sum_{k=0}^{n}(k+1)\,\alpha_{n-k}b_{k+1}$$

and

$$a_0 = 0 \qquad b_0 = 0,$$

$$\alpha_0 = 1 \qquad \beta_0 = 0,$$

$$b_1 = a_1\left(\frac{1}{2} \pm \frac{\sqrt{\epsilon(4+\epsilon)}}{2\epsilon},\right),$$

$$\lambda = 1 + \frac{\epsilon}{2} \pm \frac{\sqrt{\epsilon(4+\epsilon)}}{2}$$

and a_1 arbitrary.

If we choose the unstable eigenvalue and eigenvector (the plus sign in the formulas) we obtain the coefficients for the parametrization of the unstable manifold. Likewise choosing the stable eigenvalue and it's eigenvector (the minus sign) give the parametrization of the stable manifold. Since $x(t), \theta(t)$ are odd, a_n and b_n are zero for even n.

Are the recursion relations consistent? By this we mean, given the terms through order n, can we compute the right hand sides?

Note that

$$\sum_{k=0}^{n} (k+1)\,\beta_{n-k} b_{k+1} = \beta_n b_1 + 2\beta_{n-1} b_2 + \ldots + (n+1)\beta_0 b_{n+1}$$

$$= \beta_n b_1 + 2\beta_{n-1} b_2 + \ldots + n\beta_1 b_n$$

as $\beta_0 = 0$. However

$$\sum_{k=0}^{n} (k+1)\,\alpha_{n-k} b_{k+1} = \alpha_n b_1 + 2\alpha_{n-1} b_2 + \ldots + (n+1)\alpha_0 b_{n+1}$$

$$= \alpha_n b_1 + 2\alpha_{n-1} b_2 + \ldots + (n+1) b_{n+1}$$

as $\alpha_0 = 1$ Then, at the $n+1$-th level, α_{n+1} and β_{n+1} depend on knowing not only $\alpha_0, \ldots, \alpha_n$ and $\beta_0, \ldots, \beta_n$ but also $b_1, \ldots, b_{n+1}$. In other words, to compute the coefficients of $\sin\theta(t)$ to $n+1$-th order, we must know $\theta(t)$ to $n+1$-th order.

On the other hand

$$\sum_{k=0}^{n-1} (k+1)\,\alpha_{n-k} b_{k+1} = \alpha_n b_1 + 2\alpha_{n-1} b_2 + \ldots + [(n-1)+1]\alpha_{n-(n-1)} b_{(n-1)+1}$$

$$= \alpha_n b_1 + \alpha_{n-1} b_2 + \ldots + n\alpha_1 b_n$$

where, as was just shown above, α_n itself depends on the numbers b_i, but up to order n. Then a_{n+1} and b_{n+1} depend only on n-th order data. So, given the n-th level data, we can compute the data to order $n+1$ but the coefficients must be computed in the correct order.

The recursive computation proceeds as follows; We have α_1, β_1, a_1, and b_1. From this first order data we compute a_2 and b_2 using the recurrence relations. Once this is done we have the αs and βs to order one, and the bs to order two.

Then we compute α_2 and β_2 from their recurrence formula, at which point we have all second order data and can compute a_3 and b_3.

Inductively, if we have all data at order n for $n \geq 1$, then we can compute a_{n+1} and b_{n+1} by their recurrences. With these we have all the necessary data to compute α_{n+1} and β_{n+1}, which completes the $n+1$-th level data. By induction we can compute the coefficients to any desired finite order.

4 Numerical Results.

In this section we give some numerical results using the formula developed in the first half of the note. The first subsection shows the parameterizations for several values of ϵ. In the next section we show how the invariance equations can be cast in such a way as to allow very clear analysis of the numerical error in the computations. This will make it easy to decide when we have computed to high enough order, and when we have reached the breaking point of either our formulas, the limitations of the software, or the abilities of the machine. Finally we sketch a method which can be used to prove the existence of horseshoes in the instability zone.

4.1 Computing the Stable and Unstable Manifolds

Using these recurrence relations we can compute the stable and unstable manifolds from the origin without iterating the map. We simply compute the coefficients up to some fixed order n using the recursion scheme of the previous section, which gives the n-th order Taylor approximation $P_n(t)$ of $P(t)$. Then we can plot $P_n(t)$ to obtain a graphical representation of the stable or unstable manifold (depending on which eigenvalue and eigenvector we prime the recursion with).

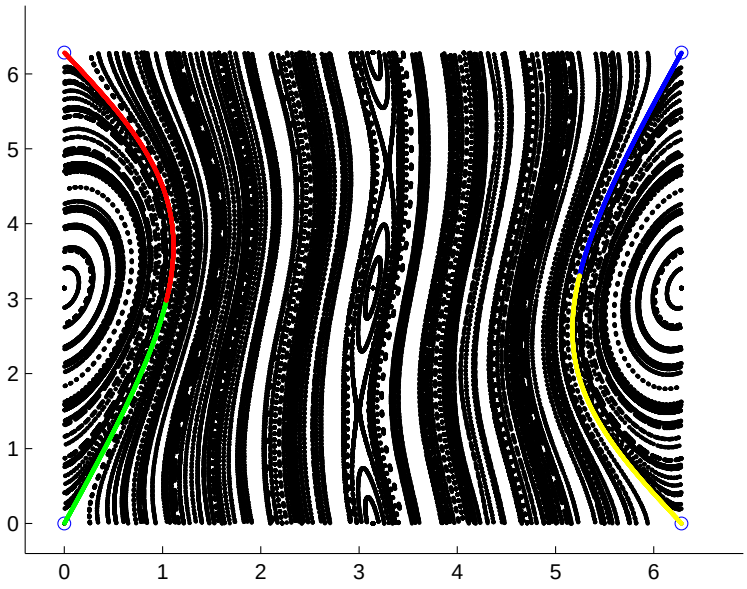

Figure 7: Parameterizations for $\epsilon = 0.3$.

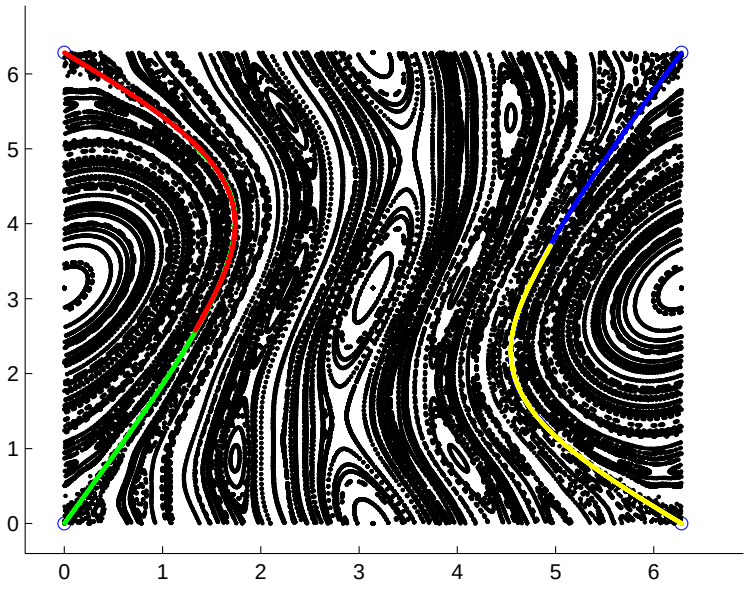

Figure 8: Parameterizations for $\epsilon = 0.7$.

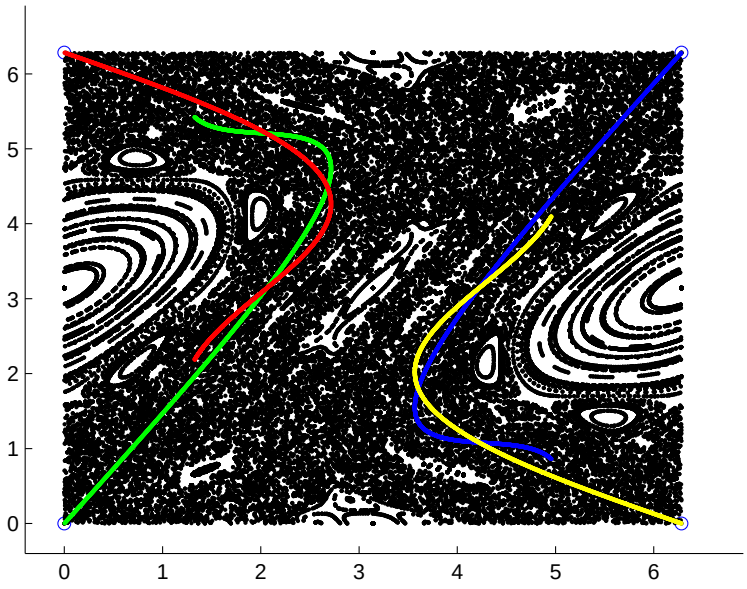

Figure 9: Parameterizations for $\epsilon = 1.5$.

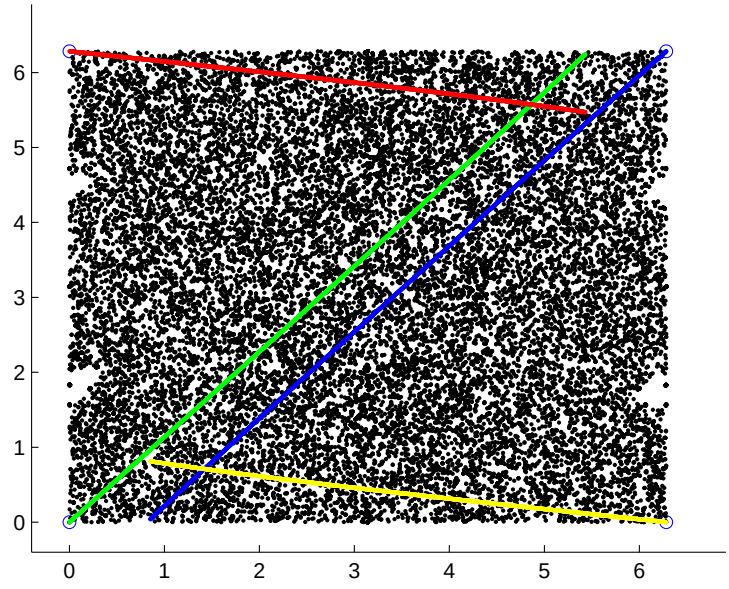

Figure 10: Parameterizations for $\epsilon = 6.5$.

Our recurrences take parameter ϵ and can be used to compute the manifolds for any $\epsilon > 0$. Figures one through four show parametric representations of the stable and unstable manifolds for four different values of epsilon. In all the figures the four corners (represented by an empty blue circle) are identified and represent the fixed point p_0. The green and blue lines are plots of the unstable manifold, green coming from the lower left corner, and blue from the upper right. The red and yellow lines are the parameterizations of the stable manifold, red coming from the upper left and yellow out of the lower right. (The left right distinctions are important later when we iterate the parameterizations).

In each of the four pictures the black points are obtained in the usual way by iterating some grid of initial conditions a few hundred times. However the colored plots of the $W(p_0)^{u,s}$ are not obtained by iterating at all. The plots are simply obtained by plugging values of t into the polynomial approximations of $P(t)$. This is in contrast to the first order methods of computing $W(p_0)^{u,s}$, where one picks a large number of values on the stable or unstable eigenvalues and very near the origin, simply iterates these, and takes the resulting orbits as an approximation of the manifolds. (Using both methods together, one can numerically estimate the accuracy of both the first order and arbitrary order methods).

By taking polynomials of order between 60 and 70 the parameterizations can be followed through several intersections of the manifolds and more than half way across the phase space. The method gives semi-local approximations as opposed to local.

Varying ϵ we see in the first two figures the characteristic "exponentially small splitting" of $W(p_0)^{u,s}$. One has to zoom in very close to see that the manifolds are not tangent. The angle between their tangent vectors at an intersection point is known to be exponentially small compared to ϵ [DR]. In the third figure many of the primary invariant circles have been broken, and the manifolds have more room to oscillate. Then we have a much clearer view of the intersections. Finally in figure four the space is almost clear of tori and the manifolds run almost straight. The dynamics are qualitatively similar to those of a hyperbolic toral automorphism.

4.2 Numerical Estimation of Error.

Our goal has been to compute a function $P : \mathbb{R} \to \mathbb{R}$ and a constant λ such that

$$(f_\epsilon \circ P)(t) = (P \circ \lambda)(t).$$

Taking λ as known, this is equivalent to asking for a root of the equation

$$(f_\epsilon \circ P)(t) - (P \circ \lambda)(t) = 0.$$

over the set of all functions P in some Banach Space. What we have found instead is a sequence of functions

$$P_N(t) = \sum_{n=1}^{N} a_n t^n$$

which we believe approximate P. Or better yet we hope that $P_n \to P$ as $n \to \infty$, again in some Banach Space (we are not over concerned with regularity here. In the literature mentioned above it is shown that under reasonable conditions P is as regular as f or in this case analytic).

Given an approximate solution $K \in C_0(U \subset \mathbb{R}, \mathbb{T}^2)$, define the error operator $E : C_0(U, \mathbb{T}^2) \to C_0(U, \mathbb{T}^2)$ by the expression

$$E(K) = f \circ K - K \circ \lambda.$$

By considering say, the $C_0(U, \mathbb{T}^2)$ norm of E, we can qualify the extent to which K is approximate. A true solution P of our problem will have $||E(P)||_{C_0} = 0$.

A proper treatment of the parametrization method involves showing that a Newton Method can be applied to the problem, and using a Nash-Moser Implicit Function Theorem to prove existence of a solution, rates of convergence, as well as *a postori* error estimates on truncation error of P_n. Again we refer to the literature.

Here, all we will show is that the error function can be used to numerically evaluate the validity of our approximations. We choose to consider an approximation P_N "good" when $||E(P_N)||_{C_0}$ is numerically less than 10^{-14}. This suggests that no point on the approximate invariant manifold is further from the actual invariant manifold then 10^{-14} (Lipschitz estimates and interval arithmetic are needed to turn suggests into implies).

Consider the plots of the stable and unstable manifold in figure 9. Recall that we had $\epsilon = 1.5$ and approximated the manifold to order 60 on a domain $U = (-11.0, 11.0)$. The graphic looks good, and if we were to compare to the first order calculation in fig 1 we would have a hard time distinguishing them.

But is the approximation "good" in the sense defined above? We give a plot of $|E(P_{60})(t)|$ for $t \in [0, 11]$ in fig 11. The horizontal axis is the parameter space and the vertical axis the norm of $E(P_{60})(t)$ in logarithmic scale. Now it is clear that our approximation is "good" until just after $t = 8.0$ but that by the time we reach the end of the manifold we only have eight significant figures.

This is more than enough to trick our eyes, and enough so that several, if not many iterations of the end of the manifold will behave properly. But it is a long way from what either the machine, or our scheme are capable of. If we want to go as far as $t = 11$ to machine accuracy, then we will have to increase the order of the calculations.

Inspired by these observations we present figure 12. Here we are doing the same approximation, for orders between 1 and 246. The horizontal axis is the parameter space again and the vertical axis is the log of the pointwise value of error functions. The first five curves (blue, green, yellow, ect) are the error functions of the P_1, ..., P_5. We see that very near the origin the error is small, but that we loose accuracy very quickly.

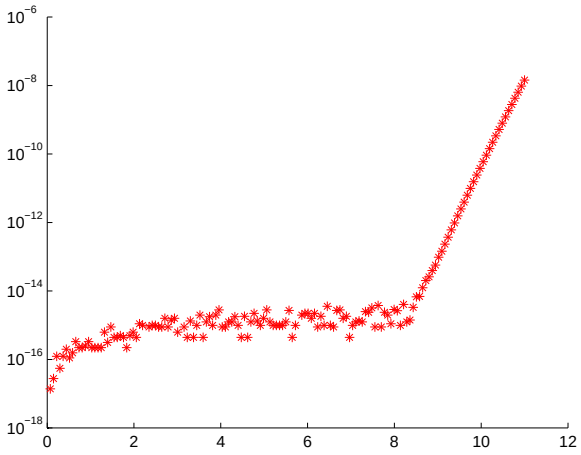

Figure 11: $|E(P_{60})(t)|$ on $[0, 11]$.

After this the curves are only plotted after the order has increased by ten. The redder the curve the higher the order. Now we begin to see that for orders between 10 and 246 we can get "good" approximations for some length of time.

The stared curve is the error function of P_{246}. We can see that by going to order 246 we obtain an approximation that is "good" until roughly $t = 15$. The plot given by this approximation is shown in figure 13. (Here we only plot 150 points of the curve. This gives the tail the thinned out look. If one wanted to fix this it's just a matter of plotting more points in an already known polynomial).

We have a very long approximation of the unstable manifold, and what is more we have validated that the approximation is good to fourteen figures right up to the end. In fact, on closer inspection we find that the error is below 10^{-15} until after $t = 8.0$ (this is well after the first intersection of the stable and unstable manifolds) and under 10^{-16} until after $t = 1.0$. For perspective if $t \in [0, 1]$ the parametrization runs through the unit square in almost a straight line, so this is still quite a long section of the manifold.

We claim that we are reaching the limit of what the MatLab can do. For orders higher than 246, MatLab returns coefficients that are zero to machine precision (The last non-zero coefficient is $a_{246} = 4.94065645841247e-324$. This is then multiplied by t^{256} to give the last term term, which is of the order of 10^{-78}).

To continue we need to implement the program in a real programming language, say $C++$ or FORTRAN. This would give access to long double precision, or if desired, multiple precision libraries like MPFUN. What is important in the present discussion is that we have a way to validate the precision of our computations, improve them if necessary, and to say when it's time to stop.

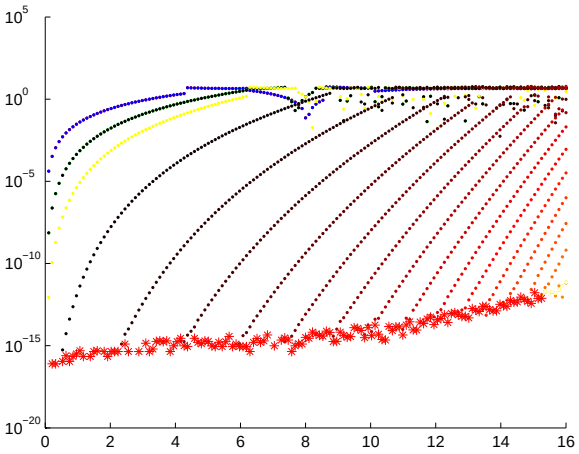

Figure 12: Error curves at orders $1 - 246$ order.

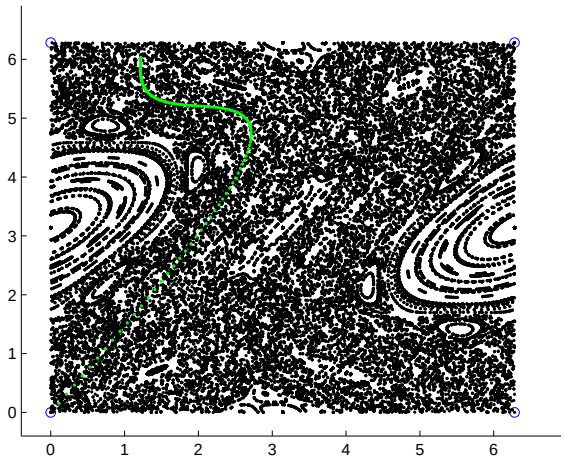

Figure 13: MatLabs Best.

As an afterthought we note that the linear analysis performed earlier can be thought of as a first order parametrization method. In this case the same error analysis applies. Examining the error function for the linear approximation we worked out in the beginning of the note, we see that for $t <= 10^{-4}$ our error is on the order of 10^{-13}. Recall that we took a thousand steps with a step size of 10^{-7}. Then the last point in our grid was on the order of 10^{-4}. This is not "good" as defined above, but it is not bad considering the trial and error nature of the approach we were taking.

If we continue the linear grid out to 10^{-2} the error is of the order of 10^{-7} and we are nowhere near the capacity of the machine. On the other hand of we wanted to apply the first order method to a grid of points that approximated the unstable manifold to sixteen figures, we could use the error function to decide how near the origin to begin (in fact this can be done by taking all grid points in a $2.5 * 10^{-5}$ neighborhood of the origin).

It should be pointed out the the linear approximation is unusually good in this system near this parameter (especially for the unstable manifold). Also, the closer your grid of points is to the origin, the slower in some sense the dynamics are. Then to get the grid away from the origin you may be required to iterate the map many times, and every iteration introduces round off error. Also, once we start iterating in any of these schemes, first order or otherwise, we no longer have the invariance equations or the error function, and it will be more difficult to estimate the validity of the resulting approximation to the invariant manifold.

4.3 Sketch of a Numerical Proof of Chaos.

Here we give an indication of how one could pursue a computer assisted proof that the map is chaotic for high enough values of ϵ (in principle any ϵ is possible, but the exponentially small splitting causes the difficulties to increase for small ϵ. Again see [DR].

The sketch is based on the "homoclinic tangle theorem"

Theorem 1 *Let $f : M \to M$ be a diffeomorphism and p be a hyperbolic fixed point of f. If $W(p)^s \cap W(p)^u$ transversally at q, then in any neighborhood of p and q there is an invariant set $S \subset M$ such that $f|_S$ is topologically conjugate to the full shift on two symbols.*

See [R] section 7.4.2 for a proof.

The existence of a subset on which a map is topologically conjugate to the shift is taken as the definition of chaos by some authors. This is called "chaos in the sense of Mischaikow" by [GN]. Conjugacy to a shift is in general easier to show that "chaos in the sense of Devaney" (sensitive to initial conditions, topologically transitive, and dense periodic orbits. See [D]). Furthermore, all systems that are known to be chaotic in the Devaney sense have been shown to be chaotic in the sense of Mischaikow. It is however not known if the definitions are equivalent. An nice discussion is in [GN].

At any rate, taking the theorem for granted what one must do is to show that the stable and unstable manifolds of the standard map intersect transversally.

While the plots in the third and fourth figures suggest this strongly all we have plotted are discrete points on the polynomial.

Further numerical evidence can be supplied by showing that the polynomial approximations of $W(p_0)^{s,u}$ actually intersect. To see this all we have to do is show that the difference of the two parametric equations (which is still polynomial) has a zero. Let $P_n^s(t)$ parameterize $W(p_0)^s$ and $P_n^u(t)$ parameterize $W(p_0)^u$ both to order n. Form

$$F(t) = P_s(t) - P_u(t) = (x_n^s(t) - x_n^u(t), \theta_n^s(t) - \theta_n^u(t)).$$

We want to prove that $F(t_0) = 0$ for some $t_0 \in U$ and that the zero is nondegenerate, i.e. $F'(t_0) \neq 0$. Then we look for simultaneous zeros of

$$F_1(t) = x_n^s(t) - x_n^u(t) \quad \text{and} \quad F_2(t) = \theta_n^s(t) - \theta_n^u(t).$$

These can be found using Newton's Method;

$$t_{n+1} = t_n - \frac{F_1(t_n)}{F_1'(t_n)}$$

$$s_{n+1} = s_n - \frac{F_2(s_n)}{F_2'(s_n)}$$

with initial condition t_0, s_0 simply read off the plot and such that the manifolds are near an intersection.

We will consider the map with $\epsilon = 1.3$ and the parametrization to order 60. A little experimentation shows that the manifolds are near an intersection when $t_0 = 5.0$ (see figure 14).

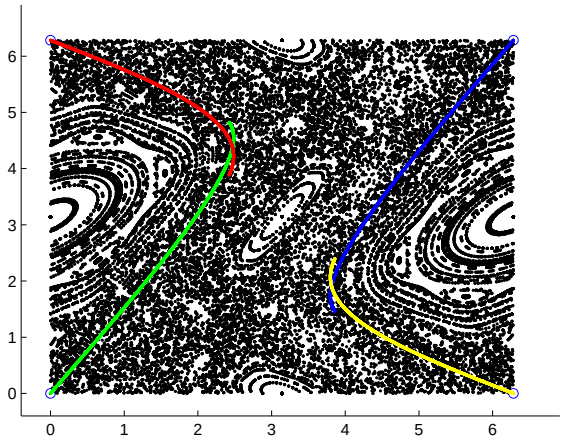

Figure 14: P([0.0, 5.0]); just past an intersection.

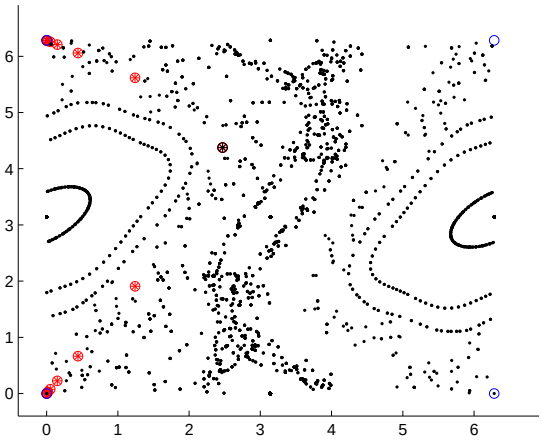

Figure 15: Forward and backward orbit of q: fifteen iterations each way.

Using this initial condition we will try to solve the Newton Iteration for a zero in the θ variables. Once this is found we will check the difference in the x variables.

Initially the difference in the θ variables is $\theta_n^u(t_0) - \theta_n^s(t_0) = 0.937$ so that our guess is fair, but certainly not great. After six steps of the Newton method we have

$$\theta_n^u(t_6) - \theta_n^s(t_6) = 0.88810^{-15}$$

with $t_6 = 3.88283666622758$. We can check that

$$x_n^u(t_6) - x_n^s(t_6) = 0.0$$

to machine accuracy. We have simultaneous zeros and a solution. Then let

$$q = (x_n^s(t_6), \theta_n^s(t_6)) = (2.46916564699772, 4.37617547708865)$$

q should be a homoclinic point to p_0. We can check this by forward and reverse iterating p.

Figure 15 shows that q is near a homoclinic orbit. The red stars show its trajectory. The black star in the middle of the trajectory is q. Fifteen iterates are shown both forward and backward. It's clear that the point goes to and from p_0.

In fact we plot the distance from the orbit to p_0 as a function of iterates in 16 to get a qualitative idea of how good an approximation q is to a homoclinic point of p. The y axis scale is log of the distance. We can see that the trajectories approach the origin for fifteen to sixteen iterates. At this point round off error

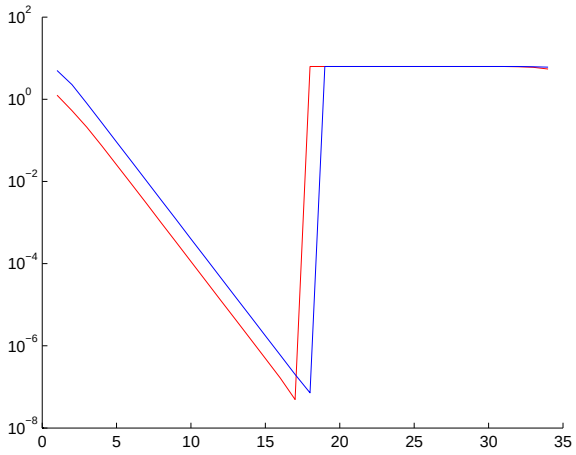

Figure 16: Log of distance to origin: Red is forward orbit, Blue reverse.

knocks them off the manifolds and they leave the origin. Nevertheless, the trajectory approaches the origin for fifteen iterates, and moves from an initial distance of order one to a distance of order 10^{-7} before diverging.

So the Newton Method produces a good approximation p to the homoclinic intersection point. To address the transversality we need to know what the derivative is there. Computing the tangent vector to each manifold at q gives

$$T(W^u)_q = \begin{bmatrix} 0.09025761967290 \\ 0.54566348852079 \end{bmatrix}$$

and

$$T(W^s)_q = \begin{bmatrix} 0.09025761967290 \\ -0.45540586884789 \end{bmatrix}$$

The angle between them is

$$\phi = 1.81352470645685 \text{ radians}$$

Equivalently, if we define a matrix T whose columns are these tangent vectors and compute its determinant we get $det(T) = -0.09035413732358$. Then the vectors span $\mathbb{R}^2$ and the intersection is transverse.

Of course this is only a sketch of the proof. For a correct proof one would carry out the computations in interval arithmetic and bound the angle or the determinant away from zero. Also, we actually only have a zero of the difference between the polynomial approximation of the manifolds. To show that there is a true zero nearby, rigorous estimates are needed on the truncation error of the

series. To prove the zero one looks for a sign change in a computation which takes round of and truncation error into account. If a similar computation bounds the angle of the tangents away from zero then one has a transverse intersection, and a proof. See [DR] for more details.

5 Appendix: Dynamics of the Standard Map

In this appendix we recall the dynamics of the standard map as a function of the parameter ϵ.

5.1 Dependance on the parameter ϵ

These plots are made by fixing and ϵ and taking a grid of 25 initial x's, and 25 initial θ's. Each of these is iterated each 200 times. The resulting figures give a nice representation of the dynamics of the system.

The first figure shows the dynamics of the unperturbed map. Here it's easy to see what is going on by hand. The map is

$$f_0(x, \theta) = (x, x + \theta)$$

Then the first component is just the identity map on x, while the second component is a circle rotation by an angle x. If x is rational then then the orbit of every θ_0 is periodic. If x is irrational then the orbit of any θ_0 fills the vertical circle densely and there are no periodic points. The $x = 0$ and $x = 2\pi$ circles are fixed.

As soon as ϵ is increased above zero, the fixed points $(0, 0)$ and $(0, \pi)$ appear. The first is hyperbolic, the second elliptic as was previously shown. For small ϵ the figure is dominated by the elliptic center behavior at $(0, \pi)$, and by the persistence of the primary tori in the middle of the figure. The primary tori develop small oscillations in the x direction. The neighborhood of the elliptic point appears to be foliated by secondary tori.

The hyperbolic fixed point at the origin will have stable and unstable manifolds, and these intersect transversally near $\theta = \pi$ so that there is a horse shoe near the boundary between the primary and secondary and hence chaotic behavior. There are also resonances amongst the secondary tori in elliptic, hyperbolic pairs. These have stable and unstable manifolds which intersect transversally as well, so that there is chaos in the regions between the primary invariant circles. However these phenomena are exponentially small with respect to ϵ, and to not appear in the second figure.

However when we increase epsilon these structures become apparent and even come to dominate. When $\epsilon = 0.3$ as in the third figure, the primary tori in the middle of the plot have broken up and been replaced by pairs of elliptic and hyperbolic fixed points with secondary tori about the elliptic points.

In the next figure with $\epsilon = 0.7$ more of the primary tori are broken and the resonance or secondary tori become the dominant feature. Further, a gap has developed between the tori about $(0, \pi)$ and the secondary tori in the middle

Figure 17: Standard Map at $\epsilon = 0$.

of the figure. In this gap the dynamics look like static. This is the Birkhoff instability zone which is filled with chaotic orbits. Here the stable and unstable manifolds of the origin give rise to horseshoes which organize the dynamics.

This trend continues as ϵ is increased. In the next two figures the primary tori completely disappear. The remaining features are the secondary tori which get smaller and smaller, and the Birkhoff instability zones increase in size. By the time $\epsilon = 1.3$ these zones are almost the entire phase space. The final few plots simply show that this trend continues, until we have almost nothing but instability. In fact it is now the remaining tori which will get exponentially small in a sea of chaos.

5.2 Numerical Visualization of the Imbedding of the Stable and Unstable Manifolds at $\epsilon = 1.3$

In this section we fix the value of ϵ at 1.3 and examine the dynamics in the instability zone. The stable and unstable manifolds intersect transversally as discussed before, giving rise to horseshoe dynamics which organize the chaotic region. What we want to do in this section is iterate the parametrization of the manifolds we computed previously to get an idea of how these horse shoes embed.

The first figure in the section shows the plot of the parameterizations at this value of ϵ. The parametrization run almost the whole height of the phase space and pass through several intersections. Now we take this set and iterate it several times. This is shown in the next several figures, and we can follow the evolution of the manifolds, and we get a very nice illustration of the way the

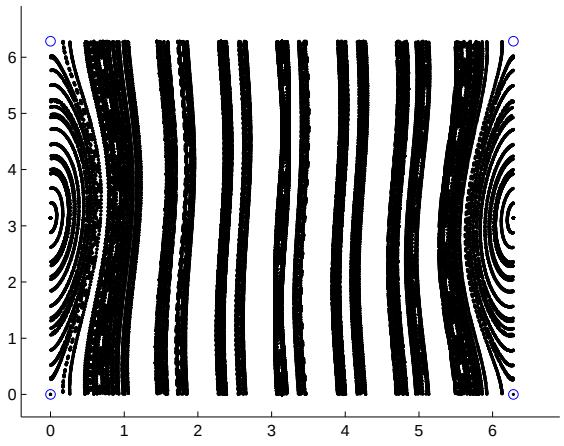

Figure 18: Standard Map at $\epsilon = 0.1$.

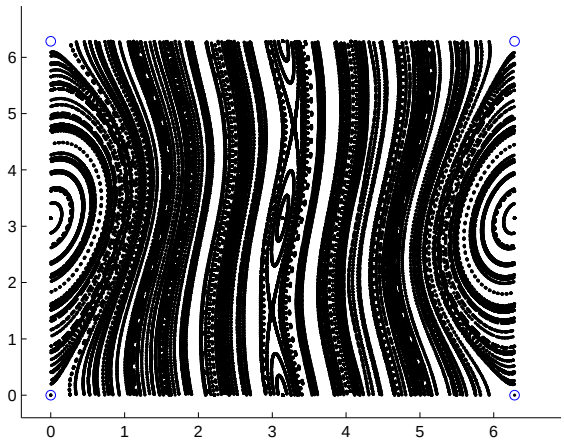

Figure 19: Standard Map at $\epsilon = 0.3$.

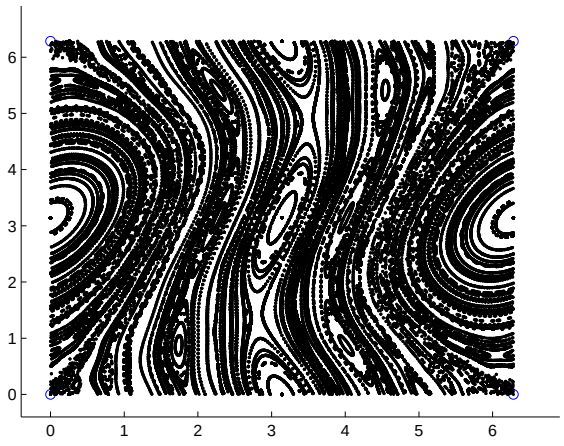

Figure 20: Standard Map at $\epsilon = 0.7$.

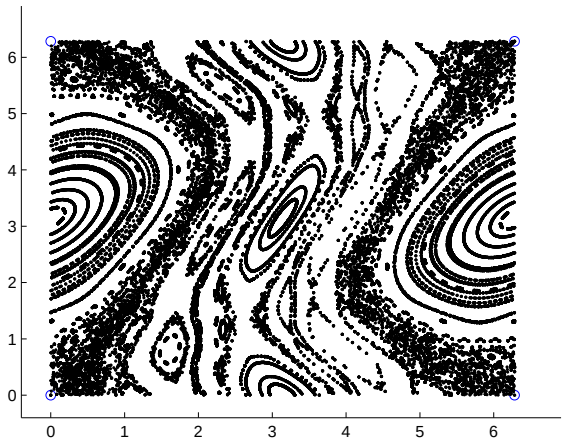

Figure 21: Standard Map at $\epsilon = 1.0$.

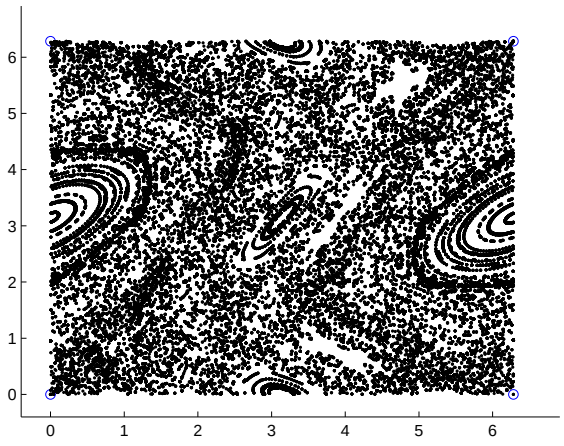

Figure 22: Standard Map at $\epsilon = 1.3$.

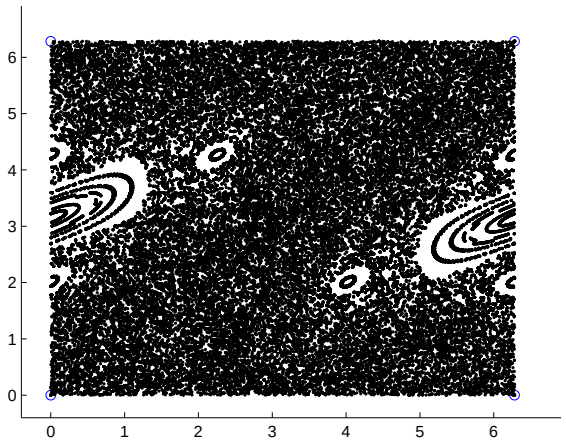

Figure 23: Standard Map at $\epsilon = 2.5$.

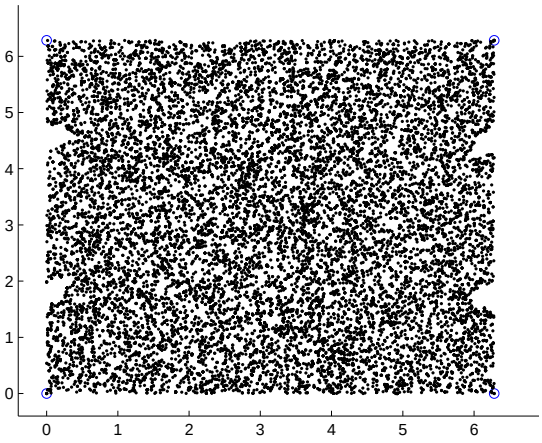

Figure 24: Standard Map at $\epsilon = 6.5$.

manifolds pile up on each other.

Figure 22 is a zoom in on crossings of the stable and unstable manifolds. The plot is reminiscent of the folding you see in the Henon attractor. Even though the manifolds are do not attract any neighborhood they give rise to the same kind of hyperbolic dynamics. The next figure is just the crossings of the iterations of the left hand side of the parameterizations.

The next two figures show the topologists sine like behavior near the origin. In the second of these we can actually see the grid like cris-crossings of the manifolds very near the origin. The closer to the origin one looks, the more the region looks like a simple grid (some of the proofs of the homoclinic tangle theorem make use of this grid structure).

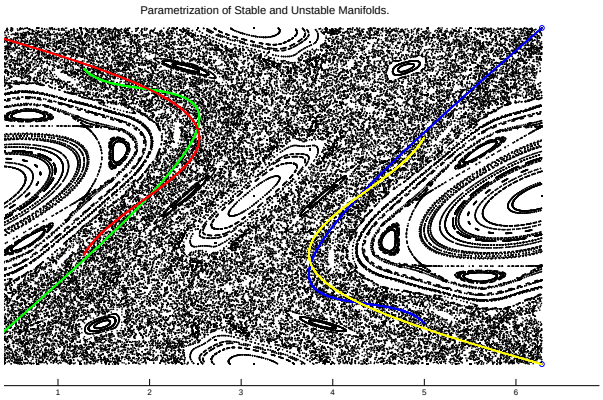

Figure 25: The graph of the parametric functions $P_{u,s}([-11.0, 11.0])$.

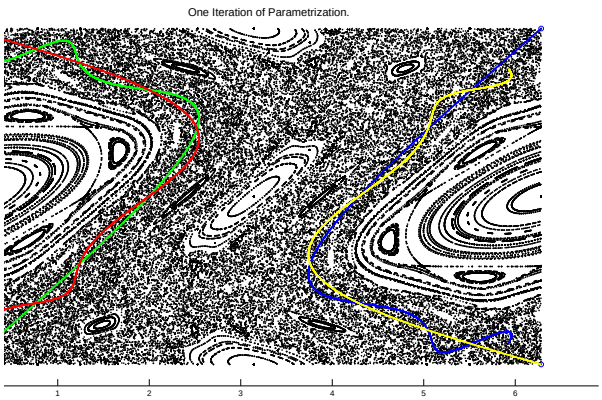

Figure 26: $f(P_u([-11.0, 11.0]))$ and $f^{-1}(P_s([-11.0, 11.0]))$.

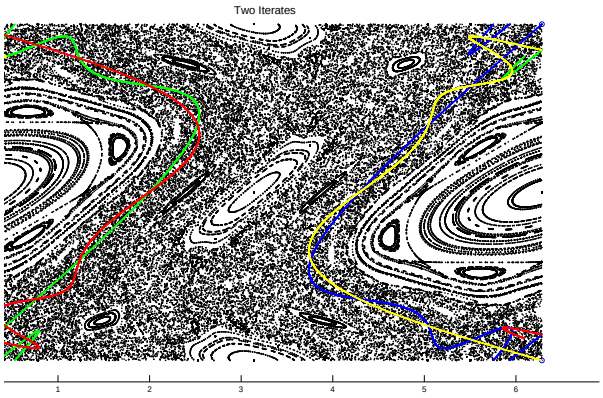

Figure 27: $f^2(P_u([-11.0, 11.0]))$ and $f^{-2}(P_s([-11.0, 11.0]))$.

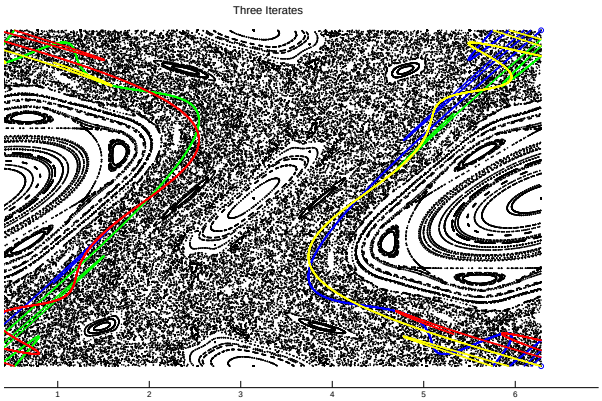

Figure 28: $f^3(P_u([-11.0, 11.0]))$ and $f^{-3}(P_s([-11.0, 11.0]))$.

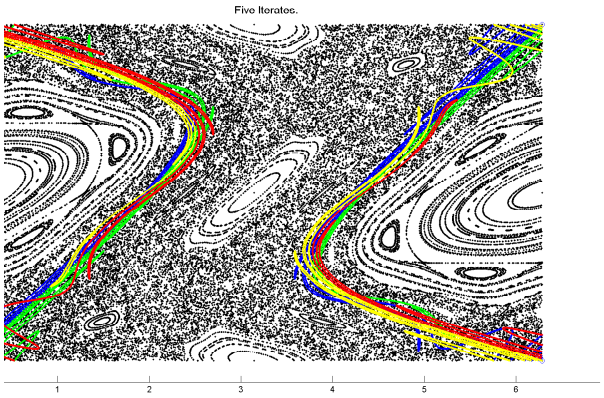

Figure 29: $f^5(P_u([-11.0, 11.0]))$ and $f^{-5}(P_s([-11.0, 11.0]))$.

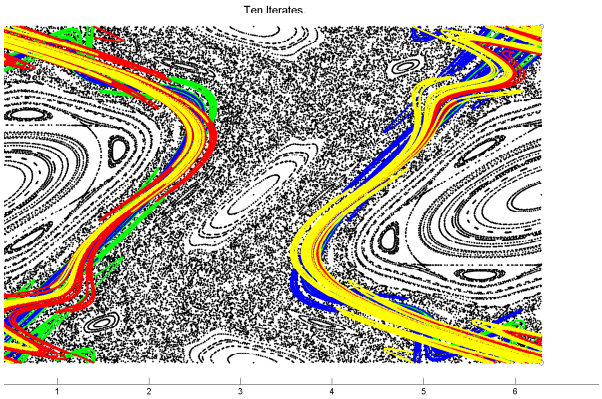

Figure 30: $f^{10}(P_u([-11.0, 11.0]))$ and $f^{-10}(P_s([-11.0, 11.0]))$.

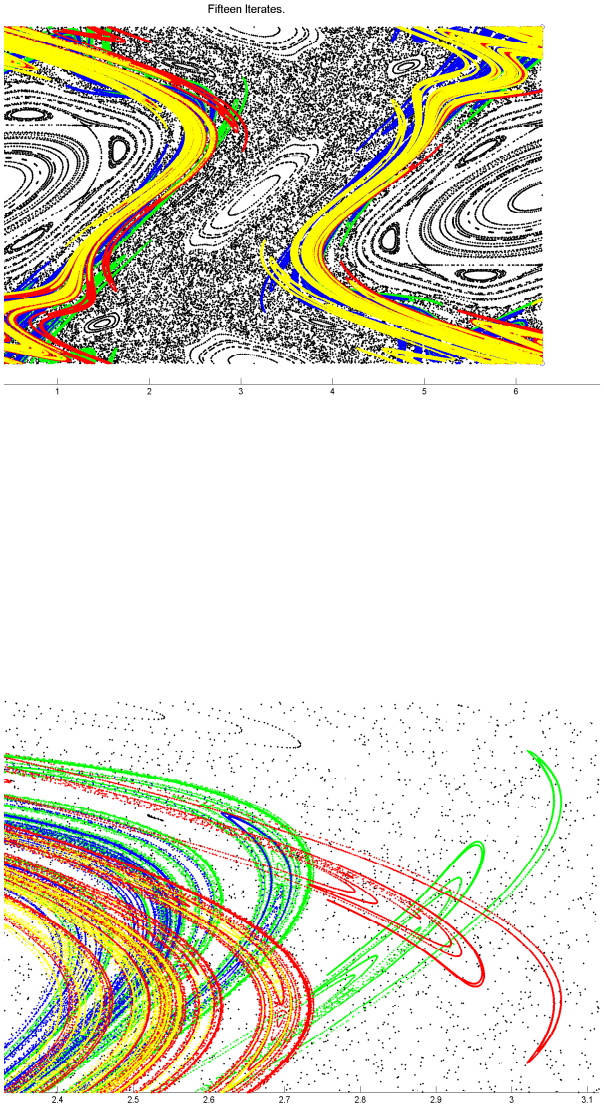

Figure 31: Near the left hand component of $W^s(O) \cap W^u(O)$.

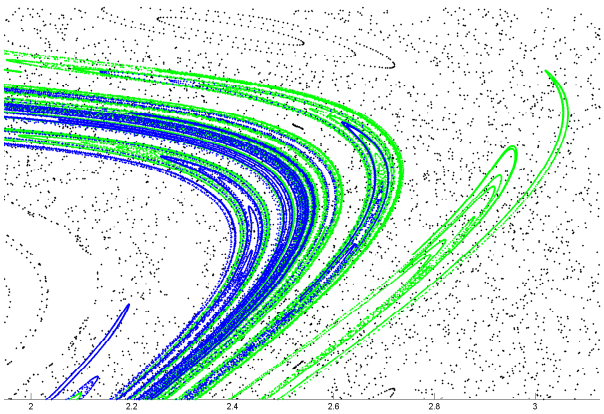

Figure 32: Parameterizations without wrapping.

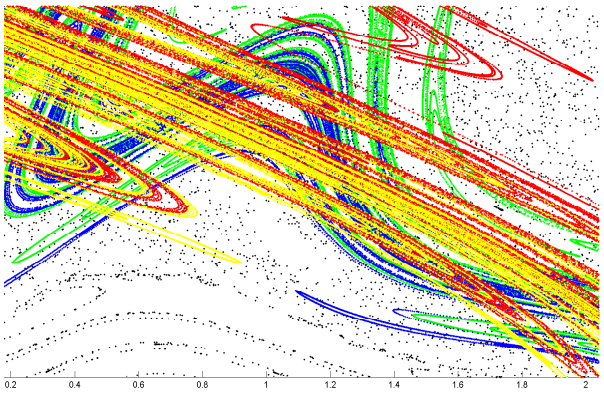

Figure 33: Pile up near origin.

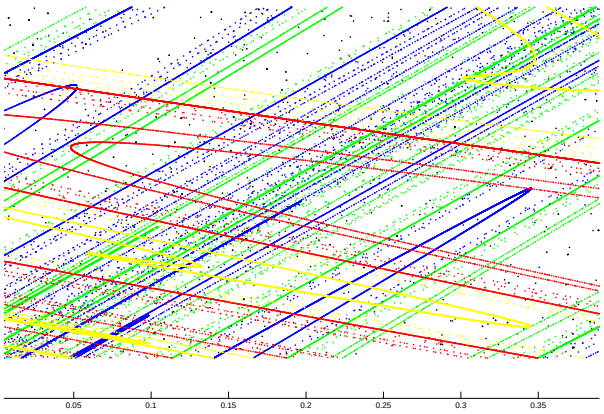

Figure 34: Checker Board near Origin.

References

[DR] "Singular separatrix splitting and the Poincare-Melnikov method for area preserving maps." Amadeu Delshams and Rafael Ramirez-Ros, Experimantal Mathematics, 8 28-48.

[HdlL1] "A Parameterization Method for the Computation of Whiskers in Quasi Periodic Maps: Rigorous Results" A Haro, R de la Llave, Preprint mparc $04-348$

[HdlL2] "A Parameterization Method for the Computation of Whiskers in Quasi Periodic Maps: Numerical Results" A Haro, R de la Llave, Preprint mparc $04-350$.

[GN] *Chaotic Dynamical Systems: An Introduction*, M Gidea, and C.P. Niculescu, University Press, Craiova, Romania.

[D] *An Introduction to Chaotic Dynamical Systems, Second Edition* R. Devaney, Westview Press, 2003

[Kun] *The Art of Computer Programming Volume 2; Seminumerical Algorithms*, D.E. Knuth, Addison-Wesley, Third Edition.

[dlL3] "KAM theory without action-angle variables" R de la Llave, A Gonzalez, A Jorba, and J Villanueva, Nonlinearity 18 (2005)

[CFdlL4] "The Parameterization Method for Invariant Manifolds I: Regularity With Respect to Parameters", X Cabre, E Fntich, R de la Llave, (Preprint)

[CFdlL5] "The Parameterization Method for Invariant Manifolds II: Manifolds Associated to Non-resonant Subspaces", X Cabre, E Fntich, R de la Llave, (Preprint)

[CFdlL5] "The Parameterization Method for Invariant Manifolds III: Overview and Applications", X Cabre, E Fntich, R de la Llave, (Preprint)

[HdlL6] "Persistence of Normally Hyperbolic Invariant Manifolds" A Haro, R de la Llave, (Preprint)

[BF] "The Parameterization Method for One-Dimensional Invariant Manifolds of Higher Dimensional Parabolic Fixed Points", I Baldoma, E Fontich, Rafael de la Llave, P Martin, Discrete and Continuous Dynamical Systems, Volume 17, Number 4, April 2007.

[MH] *Introduction to Hamiltonian Dynamical Systems and the N-body Problem,* K.R. Meyer, G.R. Hall, Springer-Verlag

[Mo] *Stable and Random Motions in Dyanamical System: With Special Emphasis on Celestial Mechanics*, Jurgen Moser, Princeton University Press, Reprint edition 2001.

[GR1] "Shadowing Orbits for Transition Chains of Invariant Tori Alternating with Birkhoff Zones of Instability", M. Gidea, C. Robinson, (preprint).

[K1] "Connecting Orbits and Invariant Manifolds in the Spatial Three-Body Problem" G. Gomez, W.S. Koon, M.W. Lo, J.E. Marsden, J. Masdemont, S.D. Ross, Nonlinearity, volume 17, issue 5, (2004)

[K2] "Invariant Manifolds, the Spatial Three-Body Problem and Petit Grand Tour of Jovian Moons", G. Gomez, W.S. Koon, M.W. Lo, J.E. Marsden, J. Masdemont, S.D Ross, Libration Point Orbits, and Applications, World Scientific (2003).

[GdlL] "Topological Methods in the Instability Problem of Hamiltonian Systems" M. Gidea, R. de la Llave, Discrete and Continuous Dynamical Systems, Vol. 14 (2006).

[GR2] "Topologically Crossing Heteroclinic Connections to Invatiant Tori" M. Gidea, C. Robinsion, Journal of Differential Equations, Vol 193 (2003).

[R] *Dynamical Systems: Stability, Symbolic Dynamics and Chaos*, Clark Robinson, Second Edition, CRC Press, Boca Raton Florida, 1999